Check for updates

Angewandte Chemie International Edition

Angewandte International Edition Chemie

How to cite: *Angew. Chem. Int. Ed.* **2026**, e9391687
doi.org/10.1002/anie.9391687

RESEARCH ARTICLE

Discovery and Characterization of Conserved N-Oxide-Forming Function of FAD-Dependent Monooxygenases for Fungal Prenylated Indole Alkaloid Biosynthesis

Tiandong Hu[1,2] | Peiyuan Feng[1,3] | Ting Lin[4] | Anran Fu[1] | Qian Wang[1,3] | Qingyu Yang[1,2] | Zechao Liu[1,3] | Shengying Li[2] | Wei Zhang[1,3,5]

[1]Laboratory of Experimental Marine Biology, Shandong Province Key Laboratory of Marine Biodiversity and Bio-resource Sustainable Utilization, Institute of Oceanology, Chinese Academy of Sciences, Qingdao, China | [2]State Key Laboratory of Microbial Technology, Shandong University, Qingdao, Shandong, China | [3]University of Chinese Academy of Science, Beijing, China | [4]School of Pharmaceutical Sciences, Fujian Provincial Key Laboratory of Innovative Drug Target Research, Xiamen University, Xiamen, China | [5]Laboratory For Marine Biology and Biotechnology, Qingdao Marine Science and Technology Center, Qingdao, China

Correspondence: Wei Zhang (weizhang@qdio.ac.cn)

Received: 12 June 2026 | **Revised:** 18 August 2026 | **Accepted:** 28 August 2026

Keywords: 3-hydroxyindolenine | flavin-dependent monooxygenase | N-oxide | prenylated indole alkaloid | stereochemistry

ABSTRACT

N-oxides are ubiquitous functional groups in natural products, conferring critical biological properties such as enhanced solubility and modulated membrane permeability. However, the biosynthetic pathways for N-oxide formation in complex prenylated indole alkaloids (PIAs), especially the penicimutamides, remain poorly understood. Here, we describe the discovery and biochemical characterization of new activities of FAD-dependent monooxygenase (FMO) PldC, which sequentially catalyzes the indole 2,3-epoxidation-rearrangement of penicimutamide E, and the regioselective N13-oxidation of penicimutamide D to produce penicimutamide D N-oxide. Furthermore, conserved N-oxide-forming activity was confirmed as a new function with another two known FMOs of CtdE and PhqK involved in the biosynthesis of citrinadins and paraherquamides, respectively. These findings provide mechanistic insights into FMO function, revealing a remarkable catalytic plasticity whereby a single enzyme family drives dual oxidative pathways (C-oxidation and N-oxidation) to generate structurally diverse alkaloid metabolites. Collectively, our findings expand the catalytic landscape of FMOs, suggesting N-oxide formation as a conserved functional trait across this enzyme family during fungal PIA biosynthesis. These results also shed new light on the evolutionary trajectories and catalytic design principles of FMOs in the assembly of complex natural products.

1 | Introduction

N-oxides (R_3N^+-O^-) represent a pharmacologically privileged and structurally widespread functional group across natural products (NPs), spanning mammalian metabolites, plant alkaloids, microbial metabolites, and marine toxins [1]. This pharmacophore is also widely found in clinically approved drugs, which possess diverse pharmacological activities [2, 3] (Figure 1A).

Tiandong Hu, Peiyuan Feng, and Ting Lin contributed equally to this work.

All rights reserved, including rights for text and data mining and training of artificial intelligence technologies or similar technologies.
© 2026 Wiley-VCH GmbH

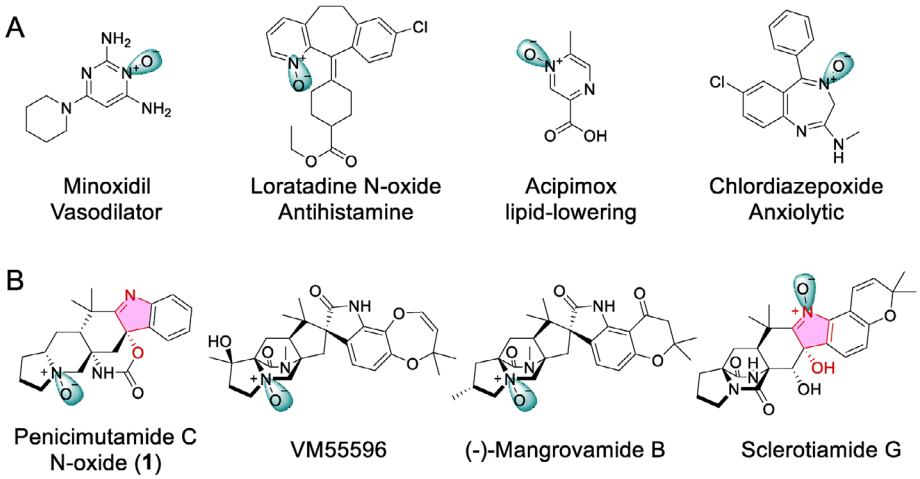


FIGURE 1 | (A) Pharmaceutical molecules containing N-heterocyclic oxides. (B) Representative fungal prenylated indole alkaloids (PIAs) with N—O coordinate bond.

Their defining polar covalent structure, characterized by charge separation between the nitrogen and oxygen atoms, confers a suite of important biological properties that shape the function of NPs and mammalian physiology alike [4]. The N-oxide moiety can enhance water solubility, improve membrane permeability, and modulate receptor binding affinity [5–7]. In ecological contexts, plant N-oxides often act as "pro-toxins" that are stored as non-toxic derivatives, they are reduced to toxic free bases upon herbivory to deter predation [8], while microbial N-oxides contribute to niche competition by inhibiting competing organisms [9].

In contract, the understanding of N-oxide biosynthesis and enzymatic mechanism remains limited. To date, only three enzyme families have been functionally linked to N-oxide biosynthesis across mammals, plants, and bacteria [10, 11]. For example, the non-heme diiron enzymes GAME33/34 generate steroidal alkaloid N-oxides in plants [12], while AurF and CmlI involved in bacterial aureothin and chloramphenicol biosynthesis [13, 14]. Cytochrome P450 of CYP71/CYP80 were found to mediate the N-oxidation of heterocyclic alkaloids of quinine and camptothecin [15]. Class A members of flavin-dependent monooxygenases (FMOs) are primarily found to catalyze the N-oxidation of simple amines, exemplified by the mammalian FMO3 and bacterial TMA monooxygenase (Tmm) in converting trimethylamine (TMA) to trimethylamine N-oxide (TMAO) [16–18], and plant senecionine N-oxygenase (SNO) in production of pyrrolizidine alkaloids [19]. Usually, FMOs can be classified into eight distinct groups (A-H) based on structural and functional diversity. Among them, Class A FMOs are single-component enzymes characterized by a conserved Rossmann-like $\beta\beta\alpha$ fold (CATH 3.50.50.60) and a D-Amino Acid Oxidase fold (CATH 3.30.9.10) [20–22].

It's worth to note, in addition to these three enzyme families found in different kingdoms, the enzyme and mechanistic basis for N-oxidation in fungal complex prenylated indole alkaloids (PIAs), one of the largest natural product families, remains underexplored [23]. During our investigation of NPs from the culture of deep-sea derived *Pallidocercospora* sp. ADS-F95, six penicimutamides belongs to subgroup of monoketopiperazine (MKP) type PIA were isolated (Figure S1A). These compounds feature a unique tetracyclic core with potential anticancer and antimicrobial activity [24–26]. Intriguingly, penicimutamide C N-oxide (**1**) features an N—O coordinate bond and a 3-hydroxyindolenine moiety. It's worth to note, an N—O coordinate bond has been identified in PIAs such as MKP VM55596 [27], (−)-mangrovamide B [28], and diketopiperazine (DKP) sclerotiamide G [29] (Figure 1B). It's also interesting to find the presence of 3-hydroxyindolenine motifs in sclerotiamide G, taichunamide A [30], speramide A [31], and asperversiamide A [32] (Figure S1B). Thus, the identification of **1** offers an ideal natural product to investigate N-oxide biosynthesis, together with 3-hydroxyindolenine motif in complex indole scaffolds.

Here, we report the discovery of bifunctional FMO PldC from *Pallidocercospora* sp. ADS-F95 that orchestrates both 3-hydroxyindolenine and N-oxidation formation. PldC first mediates the stereoselective 2,3-epoxidation of penicimutamide E (**2**) and its rearrangement to 3*S*-hydroxyindolenine (penicimutamide D, **3**), and subsequently catalyzes the regioselective N13-oxidation of **3** to generate penicimutamide D N-oxide (**4**). Notably, this N-oxide-forming activity is conserved in the indole-epoxidizing FMO homologs PhqK and CtdE, which form spirooxindoles involved in the biosynthesis of paraherquamides and citrinadins (Figure S2A), but catalyze N-oxidation of **2** and **3**, respectively. These results also for the first time demonstrate that FMO is responsible for forming the 3-hydroxyindolenine motif during the biosynthesis of PIAs. More importantly, no enzyme previously characterized for stereoselective indole epoxidation of PIAs has been shown to also catalyze N-oxidation, which is particularly striking for FMOs that specialize in indole epoxidation, further expanding the catalytic arsenal of this enzyme family in natural product diversification.

2 | Results and Discussion

2.1 | Identification of the Biosynthetic Gene Cluster of Penicimutamides

Structural elucidation revealed that compound **1** features an N—O bond and a 3-hydroxyindolenine moiety but lacks the bicy-

15213773, 0, Downloaded from https://onlinelibrary.wiley.com/doi/10.1002/anie.9391687 by Shandong University Library, Wiley Online Library on [28/09/2026]. See the Terms and Conditions (https://onlinelibrary.wiley.com/terms-and-conditions) on Wiley Online Library for rules of use; OA articles are governed by the applicable Creative Commons License

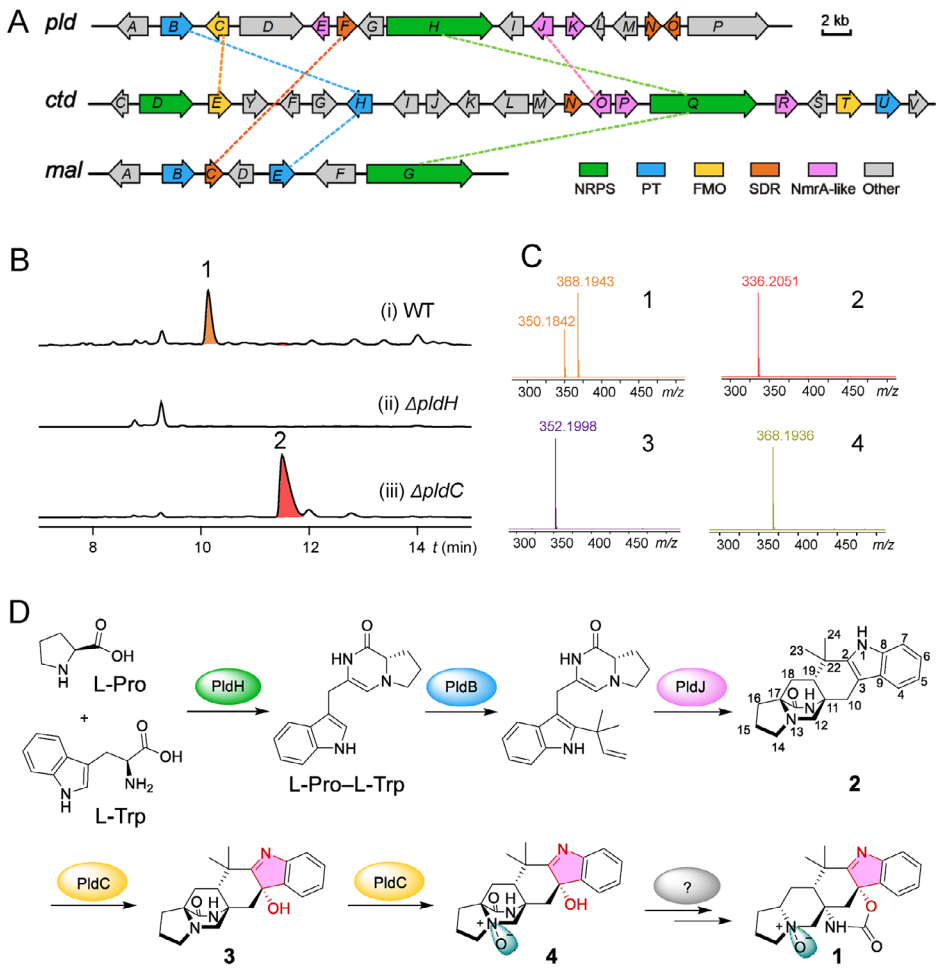


FIGURE 2 | Chemical structures, gene cluster organization, and proposed biosynthesis of the penicimutamides. (A) Comparative analysis of the biosynthetic gene clusters (BGCs) for penicimutamide C N-oxide (*pld*, from *Pallidocercospora* sp. ADS-F95), 21*R*-citrinadin A (*ctd*, from *Penicillium citrinum* ATCC 9849), and malbrancheamide (*mal*, from *Malbranchea aurantiaca* RRC1813). (B) HPLC traces ($\lambda = 280$ nm) of wild-type *Pallidocercospora* sp. ADS-F95 (WT) and the *ΔpldH* and *ΔpldC* knockout mutants. (C) LC-HRMS profiles acquired in positive electrospray ionization (ESI^+) mode. (D) Proposed biosynthetic pathway of penicimutamides.

clo[*2.2.2*]diazaoctane (BCDO) scaffold, **2** retains this ring system with the same 3*S*-hydroxyindolenine modification (Figure 2D), indicating that both share early biosynthetic steps. Typically, the first biosynthetic step of PIAs is catalyzed by a bimodular NRPS, which generates the initial dipeptide intermediate in the biosynthetic pathway. This mechanism has been reported for malbrancheamides, citrinadins, and paraherquamides [33, 34]. Using the NRPS gene *malG* from malbrancheamides biosynthesis as a probe, we identified the putative biosynthetic gene cluster (BGC) *pld* from *Pallidocercospora* sp. ADS-F95 (Figure 2A and Table S1).

To experimentally confirm the involvement of the *pld* cluster in the production of **1**, we deleted the NRPS gene *pldH* in-frame using a split-marker recombination strategy (Figure S3). High-performance liquid chromatography (HPLC) analysis showed complete abolition of **1** and other penicimutamides in the *ΔpldH* strain (Figure 2B), verifying that the *pld* is responsible for the biosynthesis of penicimutamides. Thus, PldH is responsible for the formation of cyclic $_L$-Pro–$_L$-Trp, followed by introduction of DMAPP by the prenyltransferase (PT) PldB and one of the three NmrA-like proteins (PldJ, PldE, and PldK) catalyzes the formation of BCDO scaffold (Figure 2D).

Following dipeptide backbone formation, an FMO has been proposed to catalyze indole-2,3-epoxidation during PIAs biosynthesis. Bioinformatics analysis of *pld* revealed that PldC shares homology with functionally characterized FMOs, including CtdE [34], PhqK [35], NotI [36], NotB [37], and BvnB [38] (Figure S4 and Table S2). Therefore, the encoding gene *pldC* was deleted and compound **2** ($[M+H]^+$, *obsd*. 336.2051, *calcd*. 336.2070) was accumulated as the major product, as determined via HPLC and liquid chromatography-high-resolution mass spectrometry (LC-HRMS) analyses (Figures 2B,C). Thus, PldC is identified as the candidate for the indole epoxidation, which acts after the formation of the BCDO ring (Figure 2D).

2.2 | Functional Characterization of PldC in 3-Hydroxyindole and *N*-Oxide Formation

We characterized the catalytic function of PldC in vitro using a codon-optimized *pldC* gene heterologously expressed in

15213773, 0, Downloaded from https://onlinelibrary.wiley.com/doi/10.1002/anie.9391687 by Shandong University Library, Wiley Online Library on [28/09/2026]. See the Terms and Conditions (https://onlinelibrary.wiley.com/terms-and-conditions) on Wiley Online Library for rules of use; OA articles are governed by the applicable Creative Commons License

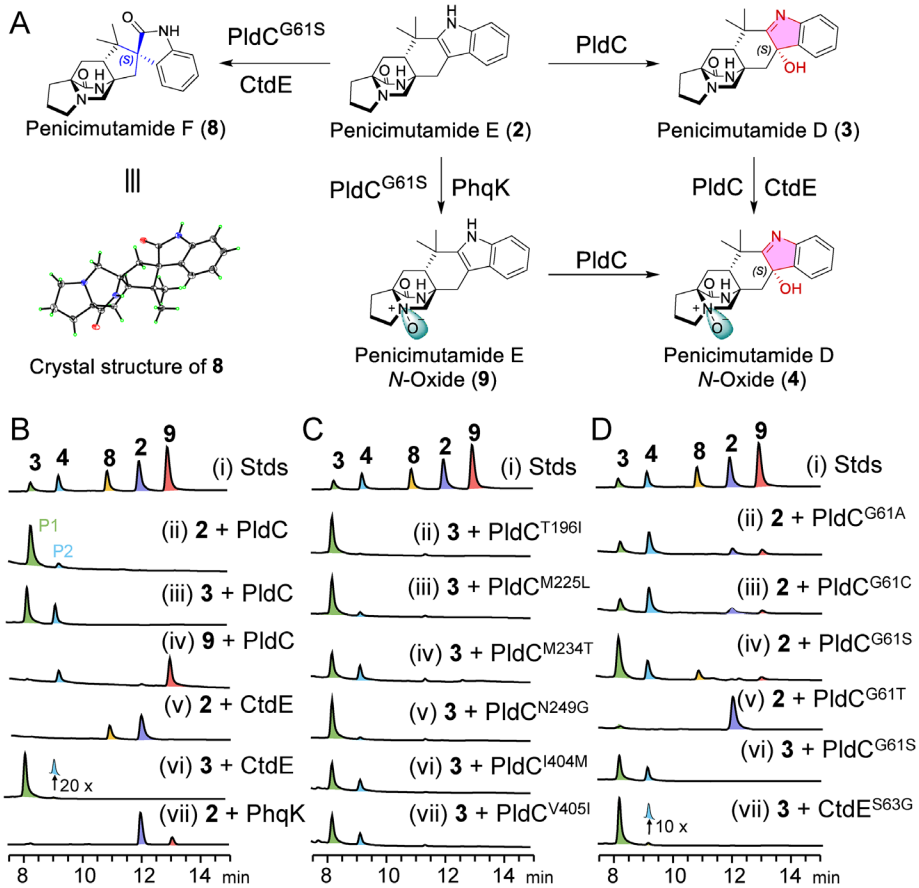


FIGURE 3 | Comparative functional characterization of PldC, CtdE, and PhqK. (A) Proposed biosynthetic pathways mediated by the three enzymes. (B, D) HPLC analysis of in vitro enzymatic reactions catalyzed by PldC, CtdE, PhqK, and their mutants using different substrates (**2**, **3**, and **9**). Stds, standards. All the chromatograms were monitored at 280 nm.

Escherichia coli BL21(DE3). The purified enzyme exhibited a bright-yellow color, and flavin analysis confirmed the binding of FAD (Figure S5) [39]. When substrate **2** was incubated with PldC in the presence of NADPH and FAD, two products, P1 and P2, were detected (Figure 3B, trace ii). The time-course analysis revealed that P1 accumulated first and was subsequently converted to P2 (Figure S6A). The incubation of purified P1 with PldC resulted in efficient formation of P2, confirming that P1 serves as an *en route* intermediate (Figure 3B, trace iii).

The chemical structure of P1 was determined to be identical to that of compound **3** ($[M+H]^+$, *obsd*. 352.1998, *calcd*. 352.2020) through integrated analysis using HPLC, LC-HRMS (Figures S7,S8), and nuclear magnetic resonance (NMR) (Figures S9,S10, and Table S7) [25]. $DP4^+$ probability and electronic circular dichroism (ECD) analysis establish P1 as compound **3**, which features a 3*S*-hydroxyindolenine scaffold (Figure S11). LC-HRMS analysis of P2 revealed a mass increase of 16 Da when compared to that of compound **3** ($[M+H]^+$, *obsd*. 368.1936, *calcd*. 368.1969), indicating a second oxidative modification (Figure S8). Comprehensive one-dimensional (1D) and two-dimensional (2D) NMR studies identified P2 as a new compound of penicimutamide D N-oxide (**4**), characterized by a distinct N-O coordination bond at N13 (Figures S12–S16 and Table S8). This N-oxide moiety was further validated by selective indium-mediated N—O bond cleavage, a mild reduction method recently developed by our group (Figure S6B) [40].

Further, isotope labeling experiments were performed to probe the oxygen origin and the catalytic mechanism. When the PldC-mediated reaction was performed in $^{18}O_2$, the molecular mass of **2** and **3** was increased by 2 and 4 Da, respectively (Figure S17). However, when the reaction was carried out in $H_2{}^{18}O$ buffer, no mass shift was observed for either product (Figure S17). Thus, O_2 is demonstrated as the oxygen source for both the N-oxide and C-oxidized products. Notably, direct N13-oxidation of substrate 2 was undetectable via both HPLC and LC-HRMS analyses, confirming that the catalytic reaction proceeds in a strict enzyme-governed sequential pathway of **2** → **3** → **4**. Michaelis–Menten kinetic analysis revealed that **2** is the preferred substrate for PldC in hydroxylation ($k_{cat}/K_M = 1.1 \pm 0.2$ min^{-1} M^{-1}), showing a 500-fold higher catalytic efficiency when compared to **3** ($k_{cat}/K_M = 2.2 \pm 0.6$ min^{-1} mM^{-1}) (Figure S18). This pronounced difference in catalytic efficiency likely accounts for the observation that **3** only accumulates after **2** has been fully consumed. These findings establish PldC as a distinctive bifunctional FMO that performs sequential oxidation of a carbenoid intermediate and a nitrogen atom, representing a rare example of dual functionality of FMOs.

2.3 | N-Oxide-Forming Activity Investigation of PldC Homologs

Thus far, few enzymes capable of catalyzing C2-C3 indole epoxidation in PIAs have been functionally characterized. Among

15213773, 0, Downloaded from https://onlinelibrary.wiley.com/doi/10.1002/anie.939168 7 by Shandong University Library, Wiley Online Library on [28/09/2026]. See the Terms and Conditions (https://onlinelibrary.wiley.com/terms-and-conditions) on Wiley Online Library for rules of use; OA articles are governed by the applicable Creative Commons License

them, CtdE, PhqK, and NotI/I' catalyze direct spirooxindole scaffold formation after the generation of the BCDO core, whereas NotB and BvnB produce 3*R*-hydroxyindoline products prior to BCDO formation [37, 38]. Notably, the substrates of CtdE and PhqK belong to the MKP family (Figure S2A), whereas those of NotI/I', NotB, and BvnB are DKP type (Figure S2B). Comparative phylogenetic analysis showed that PldC is classified into the Group A clade of FMO with CtdE and PhqK by sharing 72.4%/47.0% and 63.0%/34.7% in similarity/identity, respectively (Figure S19 and Table S2).

CtdE is known to catalyze the indole 2,3-epoxidation of (+)-precitrinadin A to form the 3*S*-spirooxindole citrinadin-5 [34]. Because **2** differs from (+)-precitrinadin A primarily by replacing the *S*-methyl pipecolate ring with a pyrrolidine ring (Figure S20), we investigated whether CtdE could accept **2** and **3** as substrates. As expected, incubating purified CtdE with **2** generated a new product, **8** ($[M+H]^+$, *obsd*. 352.2033, *calcd*. 352.2020), which is readily distinguished from **3** and **4** by its distinct UV profile and HPLC retention time (Figure 3B, trace v and Figures S5,S6). The structure of compound **8** was elucidated as a novel compound with a spirooxindole moiety by 1D and 2D NMR analysis, and designated penicimutamide F (Figures S21–S25 and Table S9). The absolute configuration of spirooxindole was unequivocally assigned as 3*S* by single-crystal x-ray diffraction analysis (Figure 3A and Table S3, CCDC 2521192). Interestingly, while CtdE cannot directly N-oxidize **2**, it converts **3** to trace amounts of N-oxide **4** (Figure 3B, trace vi).

In addition, PhqK typically catalyzes spirocyclization through two parallel pathways by transforming paraherquamide K and L into paraherquamide M and N during paraherquamide biosynthesis, and its native intermediate differs from **2** only by an *S*-methyl pyrrolidine ring (Figure S26) [35]. Driven by curiosity, we incubated the purified PhqK with **2**, surprisingly, lead to a new product (Figure 3B, trace vii). This compound was identified as the N-oxide derivative of **2** by 1D and 2D NMR analysis, featuring an N-O coordinate bond at N13, and it was accordingly designated penicimutamide E N-oxide (**9**; $[M+H]^+$, *obsd*. 352.1996, *calcd*. 352.2020; Figures S27–S32 and Table S10). The presence of the N—O coordination bond was also confirmed through an indium-mediated reductive cleavage reaction (Figure S6C). Isotope labeling experiments confirmed that the N-oxide oxygen of **9** is originated from $^{18}O_2$ (Figure S33), which is consistence to the catalytic characteristic of FMOs. However, no product was detected when **3** was used as the substrate of PhqK.

Thus, these results uncover a previously unrecognized N-oxidation capability of CtdE and PhqK (Figure 3A), two enzymes long regarded as functionally dedicated carbon-centered oxidases within the MKP family. Their dual capacity for N- and C-oxidation is modulated by substrate structure and potentially by the distinct binding modes adopted within the enzyme active pocket.

2.4 | Structural Insights Into *N*-Oxidation Function

The crystal structure of PldC was determined at 3.5 Å resolution (PDB: 26WF), however, no interpretable electron density corresponding to the FAD cofactor or bound ligand was observed (Figure S34). To further understand the catalytic mechanism of the N-oxide-forming activity, considering the high similarity of protein sequences and substrates between PldC and CtdE, we performed AlphaFold3 and molecular docking to construct structural models of PldC-FAD-**2**/**3** and CtdE-FAD-**2**/**3** based on the crystal structure of CtdE (PDB: 7KPT) (Figure S35). Structural characterization revealed that confirmed that PldC possess a Rossmann-like three-layer $\beta\beta\alpha$ sandwich domain for FAD binding, as well as a β-rich substrate-binding domain. These results confirmed that PldC belongs to canonical group A of FMOs, a family of single-component flavoenzymes distinct from other seven FMO subgroups [20–22]. In line with the classical topological features of group A FMOs, the AlphaFold3 predicted structures of PldC and CtdE exhibited highly conserved overall folding, faithfully recapitulating the defining $\beta\beta\alpha$ core architecture of this enzyme subclass. The substrate-binding cavity of each protein was enriched with hydrophobic residues, which facilitates the stable embedding of the indole ring (Figure S35).

Detailed structural analysis identified 17 residues within 5 Å of the substrate-binding site of PldC and CtdE (Figure S35); ten of these residues were conserved, while seven were divergent, including G61, T196, M225, M234, N249, I404, and V405 in PldC (corresponding to S63, I198, L227, T236, G251, M404, and I405 in CtdE). Among the differing residues, T196, M234 and N249 of PldC potentially interact with the indole unit of **2**, while G61, M225, I404, and V405 are next to the BCDO ring (Figure 4A). These interactions will lock the C2-C3 indole ring close to the C4α atom of FAD at 5.5 Å, which is suitable for the reaction. Interestingly, structural comparison revealed a difference in the spatial orientation of the FAD relative to the indole ring of substrate **2**. In PldC, FAD was located on the α-face of **2** to form 3*S*-hydroxyindolenine (Figure 4B), whereas in CtdE, FAD occupied the β-face, which drives the generation of 3*S*-spirooxindole (Figures 4C,D and S36).

The introduction of the 3-OH group of **3** is a prerequisite for the subsequent N-oxidation for PldC and CtdE. The modeling and simulations revealed that **3** adopts a conformation shifted upward relative to that of **2**, which is potentially caused by hydrogen bonds forming between the C3-OH and C20-keto groups of **3** with G334 and P331 (Figure 4E,F), respectively. This movement brings the N13 atom closer to the C4*a* (7.5 Å to 6.0 Å), optimizing the reactive distance for N-oxide formation. Furthermore, we found that the residues T196, M234, and N249 can help stabilize the productive binding mode via hydrophobic and dipole-π interactions with the indole unit of **3**. Site-directed mutagenesis revealed $PldC^{T196I}$ completely abolished the conversion of **3** to **4**, while $PldC^{M234T}$ and $PldC^{N249G}$ significantly reduced it, whereas mutating BCDO-adjacent residues (M225L, I404M, V405I) had minimal effect (Figure 3C). Importantly, none of these mutations impaired the production of **3** from **2** (Figure 4H), indicating that all mutant enzymes remained catalytical function rather than dead mutant.

In contrast, PhqK directly catalyzes N13-oxidation of substrate **2**, bypassing the 3-OH intermediate required by PldC and CtdE. Comparative molecular docking and molecular dynamics simulations revealed that the binding pose of substrate **2** in PhqK

15213773, 0, Downloaded from https://onlinelibrary.wiley.com/doi/10.1002/anie.939168 7 by Shandong University Library, Wiley Online Library on [28/09/2026]. See the Terms and Conditions (https://onlinelibrary.wiley.com/terms-and-conditions) on Wiley Online Library for rules of use; OA articles are governed by the applicable Creative Commons License

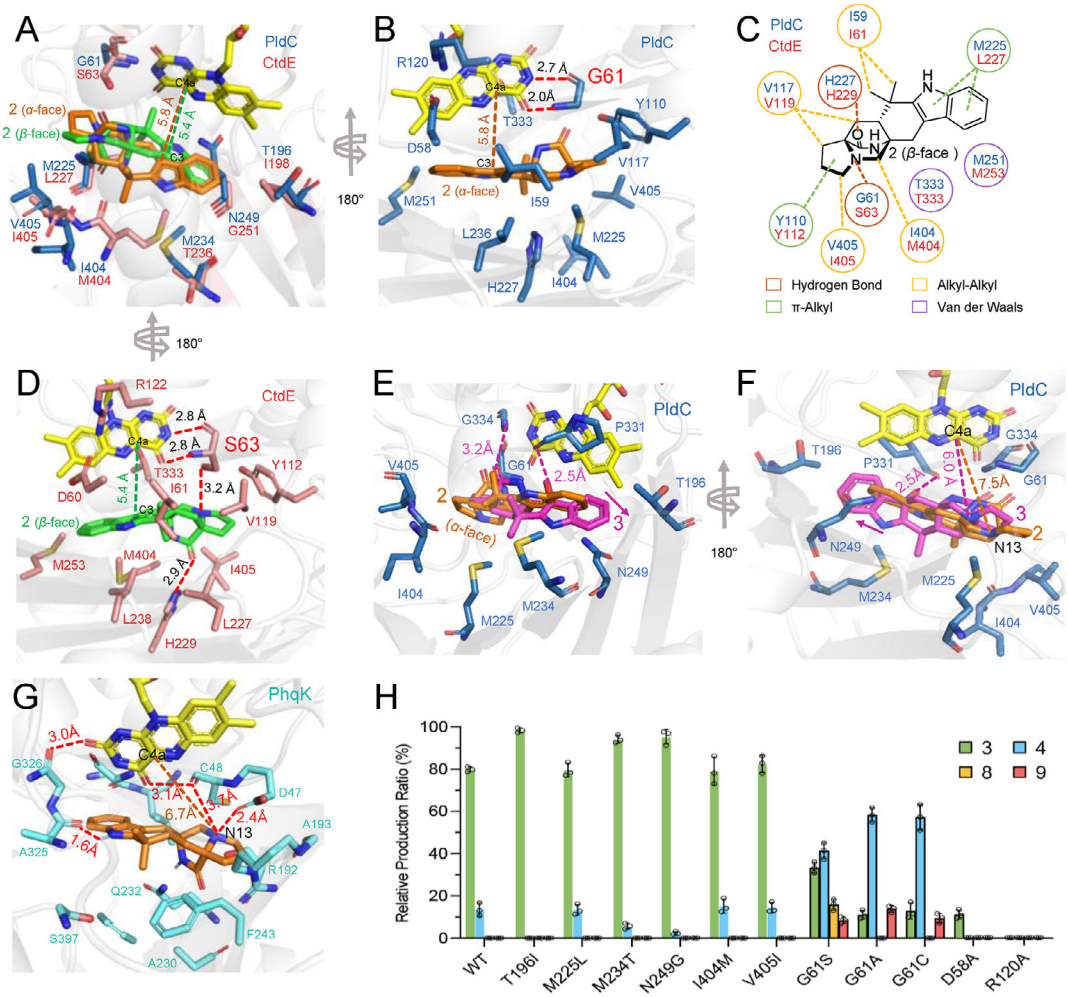


FIGURE 4 | Structural and mechanistic basis for the functional divergence between PldC and CtdE. (A) Comparison of the binding configurations of substrate **2** in PldC (skyblue) and CtdE (salmon), which are oriented for α-face (orange) and β-face (green) epoxidation, respectively. (B) PldC–FAD–**2** complexes (FAD in yellow). (C) Two-dimensional interaction diagram showing molecular contacts between substrate **2** (β-face orientation) in PldC (the corresponding amino acids are shown in skyblue) and CtdE (the corresponding amino acids are shown in salmon). (D) Active site views of the CtdE–FAD–**2**. (E,F) Superimposed binding conformations of substrate **2** (orange) and its hydroxylated derivative **3** (slate blue) within the PldC active site. (G) Binding mode of substrate **2** within PhqK (aquamarine). (H) Analysis of the relative production rate of **2** incubated with PldC and mutants. Data are presented as mean ± SD from three independent replicates.

resembles that of paraherquamide L in the PhqK crystal structure (PDB: 6PVI) [35]. Strikingly, substrate **2** adopts an approximately 180° flipped binding orientation in PhqK relative to its poses in PldC and CtdE, a divergence arising from distinct substrate-recognition interaction networks. The indole NH of **2** forms a 1.6 Å hydrogen bond with A325, rigidifying its conformation, while N13 is anchored by D47 (2.4 Å, H-bond/electrostatic) and C48 (3.7 Å, van der Waals) (Figure 4G). Residues C48 and G326 shape the catalytic microenvironment, precisely orienting N13 toward FAD. Consequently, the sterically accessible FAD C4a-OOH intermediate is positioned 6.7 Å from N13, facilitating direct N-oxide formation without the 3-OH prerequisite.

Intriguingly, while the mutations of residue G61 did not affect the ability of PldC to convert **2** to **3**, the PldC$^{G61A/S/C}$ variants directly yielded the N13-oxidation product **9** when compared to PldC^{WT} (Figures 3D and 4H). Molecular docking revealed that side chains at position 61 introduce a steric clash with the carboxy group of the substrate, forcing a downward shift that repositions N13 closer to C4*a*, thereby redirecting catalysis from C3- to N-oxidation (Figure 4F and Figure S37). In contrast, the introduction of bulkier side chains (Thr, Val, Leu, Phe, and Tyr) of this site significantly diminished enzymatic activity and completely abolished N-oxidation (Figure S38A). It's worth noting that the production of **8** is also observed with PldC^{G61S} mutant, which indicates this position is a hot-spot for the activity of PldC (Figure 3D). Furthermore, incubation of **9** with PldC yielded product **4**, while no products were detected when **9** was incubated with CtdE or its mutants (Figure 3B, trace iv and Figure S38B).

On the other hand, individual mutations of I198T, L227M, T236M, G251N, M404I, and I405V in CtdE only moderately affected the conversion of **2** to **8** (Figure S38C), and no formation of **4** was detected when the mutant enzymes were incubated with **3** (Figure S38D). In contrast, the CtdE^{S63G} completely abrogated the production of **8**, while the N-oxide-forming activity was enhanced in the CtdE^{S63G} mutant (Figure S38D). Collectively, these results

15213773, 0, Downloaded from https://onlinelibrary.wiley.com/doi/10.1002/anie.939687 by Shandong University Library, Wiley Online Library on [28/09/2026]. See the Terms and Conditions (https://onlinelibrary.wiley.com/terms-and-conditions) on Wiley Online Library for rules of use; OA articles are governed by the applicable Creative Commons License

demonstrate that within the conserved FMO pocket, substrate orientation dictates whether the peroxyflavin intermediate attacks the indole C2═C3 double bond (C—O bond) or the tertiary amine lone pair (N—O bond).

Importantly, the two ionic residues R120 and D58 in PldC are positioned adjacent to the FAD cofactor, suggesting they are potentially involved in proton transfer during the catalytic cycle and facilitating protonation for both indole epoxidation and N-oxidation (Figure S39A). As expected, the PldC^{R120A} completely abolished PldC activity toward substrate **2**, whereas the PldC^{D58A} retained only weak activity, generating minimal amounts of product **3** (Figure 4H). When PldC^{D58A} and PldC^{R120A} were individually incubated with **3**, the production of N-oxide product **4** was eliminated (Figure S38E). These results demonstrate that D58 and R120 act as strategic proton donors, playing important roles in protonation that drive both the conversion of **2** to **3** (indole 2,3-epoxidation) and **3** to **4** (N-oxidation), consistent with their proximity to FAD and the catalytic requirements of PldC. Given the considerable distance between R120 and the substrate, a bridging water molecule likely mediates proton transfer within the active site, rather than direct donation from the residues themselves. This hypothesis is supported by a bridging water molecule observed in the CtdE-FAD-citrinadin-**2** complex (Figure S39B) [34].

3 | Conclusion

In summary, our work identified the first filamentous fungal enzymes responsible for N-oxide biosynthesis in complex PIAs, revealing PldC, CtdE, and PhqK as bifunctional FMOs capable of catalyzing both indole C2-C3 epoxidation and tertiary amine N-oxidation. These enzymes were previously classified as stereoselective indole monooxygenases, and our results further indicate that their N-oxidative activity is likely evolutionarily conserved within this enzyme clade. The discovery of N-oxide-forming activity in PhqK also sheds new light on the biosynthetic assembly of VM55596 and (–)-mangrovamide B, and implies the presence of a third parallel biosynthetic route for paraherquamide-type NPs. Mechanistically, the regioselectivity toward carbon or nitrogen oxidation is predominantly dictated by substrate binding pose, rather than distinct catalytic residues or cofactor conformational rearrangement. Specifically, the substrate orients its indole C2═C3 double bond close to reactive peroxyflavin to facilitate epoxidation; by contrast, subtle repositioning of the substrate within the identical active site brings the tertiary amine nitrogen into proximity for oxygen transfer and subsequent N-oxide formation. Given the pharmacological and ecological significance of N-oxides, many functionally annotated specialized FMOs likely possess hidden N-oxygenase activity, a perspective that reshapes the current understanding of metabolic pathway evolution and oxidative diversification in natural product biosynthesis.

Author Contributions

Tiandong Hu: writing – original draft, investigation, data curation, visualization, validation. **Peiyuan Feng**: validation, data curation, investigation. **Ting Lin**: resources, data curation. **Anran Fu**: formal analysis, data curation. **Qian Wang**: software, formal analysis. **Qingyu Yang**: methodology, formal analysis. **Zechao Liu**: validation. **Shengying Li**: writing – review and editing. **Wei Zhang**: conceptualization, supervision, funding acquisition, writing – review and editing, project administration, methodology, resources.

Acknowledgments

This work was supported by the Key R&D Program of Shandong Province (2026CXPT225), the Independent Deployment Project of the Institute of Oceanology, Chinese Academy of Sciences (IOCASZZCG009), the National Natural Science Foundation of China (U2106227 and 82022066). We are grateful to the staff of the Institute of Oceanology, Chinese Academy of Sciences and the Core Facilities for Life and Environmental Sciences, State Key Laboratory of Microbial Technology of Shandong University for the LC-HRMS and NMR analyses.

Conflicts of Interest

The authors declare no conflicts of interest.

Data Availability Statement

Crystallographic data for compound **8** produced by CtdE and PldC^{G61S} have been deposited at the Cambridge Crystallographic Data Centre (CCDC) under deposition numbers 2521192 and 2521890, respectively, and can be obtained free of charge via www.ccdc.cam.ac.uk/data_request/cif. Coordinates and associated structure factors of PldC have been deposited in the Protein Data Bank (PDB) with accession code 26WF. All other experimental data supporting the findings of this study are available within the article and its Supporting Information. Source data are provided with this paper.

References

1. M. Kobus, T. Friedrich, E. Zorn, N. Burmeister, and W. Maison, "Medicinal Chemistry of Drugs With N-Oxide Functionalities," *Journal of Medicinal Chemistry* 67 (2024): 5168–5184, https://doi.org/10.1021/acs.jmedchem.4c00254.

2. A. M. Mfuh and O. V. Larionov, "Heterocyclic N-Oxides—An Emerging Class of Therapeutic Agents," *Current Medicinal Chemistry* 22 (2015): 2819–2857, https://doi.org/10.2174/0929867322666150619104007.

3. G. F. dos Santos Fernandes, P. C. de Souza, E. Moreno-Viguri, et al., "Design, Synthesis, and Characterization of N-Oxide-Containing Heterocycles With In Vivo Sterilizing Antitubercular Activity," *Journal of Medicinal Chemistry* 60 (2017): 8647–8660, https://doi.org/10.1021/acs.jmedchem.7b01332.

4. K. Ma, T. Qi, L. Hu, et al., "Atroposelective Synthesis of Biaryl N -Oxides via Cu-Catalyzed De Novo Heteroaromatic N -Oxide Ring Formation," *Advanced Science* 11 (2024): e2405743, https://doi.org/10.1002/advs.202405743.

5. F. Widjaja, L. Zheng, S. Wesseling, and I. Rietjens, "Physiologically Based Kinetic Modeling of Senecionine N-Oxide in Rats as a New Approach Methodology to Define the Effects of Dose and Endpoint Used on Relative Potency Values of Pyrrolizidine Alkaloid N-Oxides," *Frontiers in Pharmacology* 14 (2023): 1125146, https://doi.org/10.3389/fphar.2023.1125146.

6. X. F. Shang, S. L. Morris-Natschke, Y. Q. Liu, et al., "Biologically Active Quinoline and Quinazoline Alkaloids Part I," *Medicinal Research Reviews* 38 (2018): 775–828, https://doi.org/10.1002/med.21466.

7. C. Fan, F. Zhou, W. Huang, et al., "Characterization of an Efficient N-Oxygenase From Saccharothrix sp. and Its Application in the Synthesis of Azomycin," *Biotechnology for Biofuels and Bioproducts* 16 (2023): 194, https://doi.org/10.1186/s13068-023-02446-5.

8. R. Lindigkeit, A. Biller, M. Buch, H. M. Schiebel, M. Boppré, and T. Hartmann, "The Two Faces of Pyrrolizidine Alkaloids: The Role of the

15213773, 0, Downloaded from https://onlinelibrary.wiley.com/doi/10.1002/anie.939168 7 by Shandong University Library, Wiley Online Library on [28/09/2026]. See the Terms and Conditions (https://onlinelibrary.wiley.com/terms-and-conditions) on Wiley Online Library for rules of use; OA articles are governed by the applicable Creative Commons License

Tertiary Amine and Its N -Oxide in Chemical Defense of Insects With Acquired Plant Alkaloids," *European Journal of Biochemistry* 245 (1997): 626–636, https://doi.org/10.1111/j.1432-1033.1997.00626.x.

9. M. Zhang, L. Zhang, J. Li, et al., "Nitrogen-Shaped Microbiotas With Nutrient Competition Accelerate Early-Stage Residue Decomposition in Agricultural Soils," *Nature Communications* 16 (2025): 5793, https://doi.org/10.1038/s41467-025-60948-2.

10. G. L. Morgan and B. Li, "In Vitro Reconstitution Reveals a Central Role for the N-Oxygenase PvfB in (Dihydro)Pyrazine- N -Oxide and Valdiazen Biosynthesis," *Angewandte Chemie International Edition* 59 (2020): 21387–21391, https://doi.org/10.1002/anie.202005554.

11. L. Yang, Z. Pu, J. Wu, et al., "Regulating the N-Oxidation Selectivity of P450BM3 Monooxygenases for N-Heterocycles Through Computer-Assisted Structure-Guided Design," *Nature Communications* 16 (2025): 6494, https://doi.org/10.1038/s41467-025-61773-3.

12. W. Zhu, J. A. Buffa, Z. Wang, et al., "Flavin Monooxygenase 3, the Host Hepatic Enzyme in the Metaorganismal Trimethylamine N-Oxide-Generating Pathway, Modulates Platelet Responsiveness and Thrombosis Risk," *Journal of Thrombosis and Haemostasis* 16 (2018): 1857–1872, https://doi.org/10.1111/jth.14234.

13. Y. Chen, N. A. Patel, A. Crombie, J. H. Scrivens, and J. C. Murrell, "Bacterial Flavin-containing Monooxygenase is Trimethylamine Monooxygenase," *Proceedings of the National Academy of Sciences of the United States of America* 108 (2011): 17791–17796, https://doi.org/10.1073/pnas.1112928108.

14. C. Y. Li, X. L. Chen, D. Zhang, et al., "Structural Mechanism for Bacterial Oxidation of Oceanic Trimethylamine Into Trimethylamine N -Oxide," *Molecular Microbiology* 103 (2017): 992–1003, https://doi.org/10.1111/mmi.13605.

15. C. Naumann, T. Hartmann, and D. Ober, "Evolutionary Recruitment of a Flavin-Dependent Monooxygenase for the Detoxification of Host Plant-Acquired Pyrrolizidine Alkaloids in the Alkaloid-Defended Arctiid Moth Tyria Jacobaeae," *Proceedings of the National Academy of Sciences of the United States of America* 99 (2002): 6085–6090, https://doi.org/10.1073/pnas.082674499.

16. P. D. Sonawane, A. Jozwiak, R. Barbole, et al., "2-Oxoglutarate-Dependent Dioxygenases Drive Expansion of Steroidal Alkaloid Structural Diversity in the Genus Solanum," *New Phytologist* 234 (2022): 1394–1410, https://doi.org/10.1111/nph.18064.

17. H. Lu, E. Chanco, and H. Zhao, "CmlI Is an N-Oxygenase in the Biosynthesis of Chloramphenicol," *Tetrahedron* 68 (2012): 7651–7654, https://doi.org/10.1016/j.tet.2012.06.036.

18. M. Simurdiak, J. Lee, and H. Zhao, "A New Class of Arylamine Oxygenases: Evidence That p -Aminobenzoate N- Oxygenase (AurF) Is a Di-Iron Enzyme and Further Mechanistic Studies," *ChemBioChem* 7 (2006): 1169–1172, https://doi.org/10.1002/cbic.200600136.

19. T. D. Nguyen and T. T. Dang, "Cytochrome P450 Enzymes as Key Drivers of Alkaloid Chemical Diversification in Plants," *Frontiers in Plant Science* 12 (2021): 682181, https://doi.org/10.3389/fpls.2021.682181.

20. N. Polidori, G. Catucci, S. J. Sadeghi, and G. Gilardi, "Class A Flavoprotein Monooxygenases: Checkpoint and New Horizons," *Biotechnology Advances* 83 (2025): 108651, https://doi.org/10.1016/j.biotechadv.2025.108651.

21. Y. Li, L. Zhao, X. Pu, et al., "Flavin-Dependent Monooxygenases as Versatile Biocatalysts in Biomanufacturing: Mechanisms, Engineering, and Applications," *Biotechnology for Biofuels and Bioproducts* 19 (2026): 42, https://doi.org/10.1186/s13068-026-02755-5.

22. A. Phintha and P. Chaiyen, "Unifying and Versatile Features of Flavin-Dependent Monooxygenases: Diverse Catalysis by a Common C4a-(hydro)peroxyflavin," *Journal of Biological Chemistry* 299 (2023): 105413, https://doi.org/10.1016/j.jbc.2023.105413.

23. L. Du, L. Dian, S. A. Newmister, et al., "The Mutually Inspiring Biological and Chemical Synthesis of Fungal Bicyclo[2.2.2]Diazaoctane Indole Alkaloids," *Chemical Reviews* 125 (2025): 1718–1804, https://doi.org/10.1021/acs.chemrev.4c00250.

24. C. W. Li, C. J. Wu, C. B. Cui, L. L. Xu, F. Cao, and H. J. Zhu, "Penicimutamides A–C: Rare Carbamate-Containing Alkaloids From a Mutant of the Marine-Derived *Penicillium Purpurogenum* G59," *RSC Advances* 6 (2016): 73383–73387, https://doi.org/10.1039/c6ra14904a.

25. C. J. Wu, C. W. Li, H. Gao, X. J. Huang, and C. B. Cui, "Penicimutamides D-E: Two New Prenylated Indole Alkaloids From a Mutant of the Marine-Derived *Penicillium Purpurogenum* G59," *RSC Advances* 7 (2017): 24718–24722, https://doi.org/10.1039/c7ra02446k.

26. S. Gao, X. Lin, Y. Shi, et al., "A New Hypoglycemic Prenylated Indole Alkaloid N-Oxide From Endophytic Fungus *Pallidocercospora* Crystalline," *International Journal of Molecular Sciences* 24 (2023): 8767, https://doi.org/10.3390/ijms24108767.

27. R. M. Williams, J. F. Sanz-Cervera, F. Sancenón, J. A. Marco, and K. M. Halligan, "Biomimetic Diels–Alder Cyclizations for the Construction of the Brevianamide, Paraherquamide, Sclerotamide, Asperparaline and VM55599 Ring Systems," *Bioorganic & Medicinal Chemistry* 6 (1998): 1233–1241, https://doi.org/10.1016/s0968-0896(98)00102-3.

28. B. Yang, J. Dong, X. Lin, X. Zhou, Y. Zhang, and Y. Liu, "New Prenylated Indole Alkaloids From Fungus *Penicillium* sp. derived of Mangrove Soil Sample," *Tetrahedron* 70 (2014): 3859–3863, https://doi.org/10.1016/j.tet.2014.04.043.

29. X. Guo, Q. Meng, J. Liu, et al., "Sclerotiamides C–H, Notoamides From a Marine Gorgonian-Derived Fungus With Cytotoxic Activities," *Journal of Natural Products* 85 (2022): 1067–1078, https://doi.org/10.1021/acs.jnatprod.1c01194.

30. F. Li, Z. Zhang, G. Zhang, et al., "Determination of Taichunamide H and Structural Revision of Taichunamide A," *Organic Letters* 20 (2018): 1138–1141, https://doi.org/10.1021/acs.orglett.8b00061.

31. Y. W. Chang, C. M. Yuan, J. Zhang, et al., "Speramides A–B, Two New Prenylated Indole Alkaloids From the Freshwater-Derived Fungus Aspergillus Ochraceus KM007," *Tetrahedron Letters* 57 (2016): 4952–4955, https://doi.org/10.1016/j.tetlet.2016.09.071.

32. H. Li, W. Sun, M. Deng, et al., "Asperversiamides, Linearly Fused Prenylated Indole Alkaloids From the Marine-derived Fungus Asperversiamides, Linearly Fused Prenylated Indole Alkaloids From the Marine-Derived Fungus Aspergillus *Versicolor*," *Journal of Organic Chemistry* 83 (2018): 8483–8492, https://doi.org/10.1021/acs.joc.8b01087.

33. Q. Dan, S. A. Newmister, K. R. Klas, et al., "Fungal Indole Alkaloid Biogenesis Through Evolution of a Bifunctional Reductase/Diels–Alderase," *Nature Chemistry* 11 (2019): 972–980, https://doi.org/10.1038/s41557-019-0326-6.

34. Z. Liu, F. Zhao, B. Zhao, et al., "Structural Basis of the Stereoselective Formation of the Spirooxindole Ring in the Biosynthesis of Citrinadins," *Nature Communications* 12 (2021): 4158, https://doi.org/10.1038/s41467-021-24421-0.

35. A. E. Fraley, K. C. Haatveit, Y. Ye, et al., "Molecular Basis for Spirocycle Formation in the Paraherquamide Biosynthetic Pathway," *Journal of the American Chemical Society* 142 (2020): 2244–2252, https://doi.org/10.1021/jacs.9b09070.

36. A. E. Fraley, H. T. Tran, S. P. Kelly, et al., "Flavin-Dependent Monooxygenases NotI and NotI′ Mediate Spiro-Oxindole Formation in Biosynthesis of the Notoamides," *ChemBioChem* 21 (2020): 2449–2454, https://doi.org/10.1002/cbic.202000004.

37. S. Y. Li, J. M. Finefield, J. D. Sunderhaus, T. J. McAfoos, R. M. Williams, and D. H. Sherman, "Biochemical Characterization of NotB as an FAD-Dependent Oxidase in the Biosynthesis of Notoamide Indole Alkaloids," *Journal of the American Chemical Society* 134 (2012): 788–791, https://doi.org/10.1021/ja3107753.

38. Y. Ye, L. Du, X. Zhang, et al., "Fungal-Derived Brevianamide Assembly by a Stereoselective Semipinacolase," *Nature Catalysis* 3 (2020): 497–506, https://doi.org/10.1038/s41929-020-0454-9.

15213773, 0, Downloaded from https://onlinelibrary.wiley.com/doi/10.1002/anie.939687 by Shandong University Library, Wiley Online Library on [28/09/2026]. See the Terms and Conditions (https://onlinelibrary.wiley.com/terms-and-conditions) on Wiley Online Library for rules of use; OA articles are governed by the applicable Creative Commons License

39. A. Aliverti, B. Curti, and M. A. Vanoni, "Identifying and Quantitating FAD and FMN in Simple and in Iron-Sulfur-Containing Flavoproteins," *Methods in Molecular Biology* 131 (1999): 9–23, https://doi.org/10.1385/1-59259-266-x:9.

40. S. Cicchi, M. Bonanni, F. Cardona, J. Revuelta, and A. Goti, "Indium-Mediated Reduction of Hydroxylamines to Amines," *Organic Letters* 5 (2003): 1773–1776, https://doi.org/10.1021/ol034434l.

Supporting Information

Additional supporting information can be found online in the Supporting Information section.

Supporting File: anie74699-sup-0001-SuppMat.docx.

15213773, 0, Downloaded from https://onlinelibrary.wiley.com/doi/10.1002/anie.9391687 by Shandong University Library, Wiley Online Library on [28/09/2026]. See the Terms and Conditions (https://onlinelibrary.wiley.com/terms-and-conditions) on Wiley Online Library for rules of use; OA articles are governed by the applicable Creative Commons License